Article

SOURCE DATA | TRANSPARENT PROCESS

THE EMBO JOURNAL

Mechanism of formate–nitrite transporters by dielectric shift of substrate acidity

Marie Wiechert & Eric Beitz*

Abstract

Bacterial formate–nitrite transporters (FNTs) regulate the metabolic flow of small, weak mono-acids. Recently, the eukaryotic PfFNT was identified as the malaria parasite's lactate transporter and novel drug target. Despite crystal data, central mechanisms of FNT gating and transport remained unclear. Here, we show elucidation of the FNT transport mechanism by single-step substrate protonation involving an invariant lysine in the periplasmic vestibule. Opposing earlier gating hypotheses and electrophysiology reports, quantification of total uptake by radiolabeled substrate indicates a permanently open conformation of the bacterial formate transporter, FocA, irrespective of the pH. Site-directed mutagenesis, heavy water effects, mathematical modeling, and simulations of solvation imply a general, proton motive force-driven FNT transport mechanism: Electrostatic attraction of the acid anion into a hydrophobic vestibule decreases substrate acidity and facilitates protonation by the bulk solvent. We define substrate neutralization by proton transfer for transport via a hydrophobic transport path as a general theme of the Amt/Mep/Rh ammonium and formate–nitrite transporters.

Keywords formate–nitrite transporter; lactate; neutralization; proton transfer; transport mechanism

Subject Categories Microbiology, Virology & Host Pathogen Interaction; Structural Biology

DOI 10.15252/embj.201695776 | Received 22 September 2016 | Revised 25 January 2017 | Accepted 30 January 2017 | Published online 1 March 2017

The EMBO Journal (2017) 36: 949–958

Introduction

Weak acid transporters of the formate–nitrite transporter family (FNT) are key regulators of the metabolic flow in microorganisms (Lü *et al*, 2013). The formate transporter (FocA) enables bacterial growth under anaerobic mixed acid fermentation conditions by acting as an outward transporter; in the inward direction, FocA fuels the energy generating formate hydrogen lyase reaction (Suppmann & Sawers, 1994; Sawers, 2005, 2006; Kim *et al*, 2010; Lü *et al*, 2012a). Nitrite as derived from chemical reduction of nitrate or oxidation of nitrogen monoxide is transported via NirC (Jia *et al*, 2009; Clegg *et al*, 2012; Lü *et al*, 2012b). Nitrite depletion due to rapid uptake by *Salmonella* species allows the bacteria to evade killing by activated macrophages of the infected host rendering NirC a virulence factor (Das *et al*, 2009). Subsequently, a bacterial hydrosulfide transporter, HSC, was added to the FNT family (Czyzewski & Wang, 2012). Most recently, we identified the lactic acid transporting *Plasmodium falciparum* PfFNT as a vital component of the malaria parasite's energetic flux (Marchetti *et al*, 2015; Wu *et al*, 2015). Based on their critical roles in microorganisms and absence in humans, FNTs are considered potential drug targets, in particular against infections with *Salmonella* (Das *et al*, 2009) and malaria parasites (Marchetti *et al*, 2015; Wu *et al*, 2015).

High-resolution FNT crystal data (Wang *et al*, 2009; Waight *et al*, 2010; Lü *et al*, 2011, 2012b; Czyzewski & Wang, 2012) revealed a common homopentameric structure composed of five aquaporin-like, individual transporting units. FNT protomers consist of six transmembrane spans with the termini at the cytoplasmic side. The substrate path is occluded by two hydrophobic constrictions, which sandwich the imidazole side chain of a highly conserved histidine (Fig 1A; position 209 in FocA, and 230 in PfFNT).

Despite ample structure information, key questions remain unresolved and debated concerning FNT selectivity, gating, and transport (Waight *et al*, 2010, 2013; Lü *et al*, 2013; Lv *et al*, 2013). A substrate discriminating selectivity filter site has not been described, probably because the preference of bacterial FNTs for formate, nitrate, or hydrosulfide was evident from the genetic context of the transporter-encoding genes (Lü *et al*, 2013). Regarding the FNT transport mechanism, it is unclear whether the acid anion substrate, for example, formate, is required to be neutralized to pass the hydrophobic constriction sites (Lü *et al*, 2013; Waight *et al*, 2013). The central histidine (Fig 1A) was found to be essential for functionality and has been suggested to act as a site of substrate protonation. It is further hypothesized that the transferred proton can be relayed back from the neutralized substrate to the histidine via a threonine residue and a fixed water molecule after passing the constrictions (electrogenic anion transport). Alternatively, the proton may leave the protein together with the substrate anion after the passage (electroneutral anion/proton symport). Even a pH-sensitive gating mechanism is proposed involving the N-terminal domain as well as a switch in functionality from anion transport to anion/proton symport (Lü *et al*, 2011).

Department of Pharmaceutical and Medicinal Chemistry, Christian-Albrechts-University of Kiel, Kiel, Germany
*Corresponding author. Tel: +49 431 880 1809; E-mail: ebeitz@pharmazie.uni-kiel.de

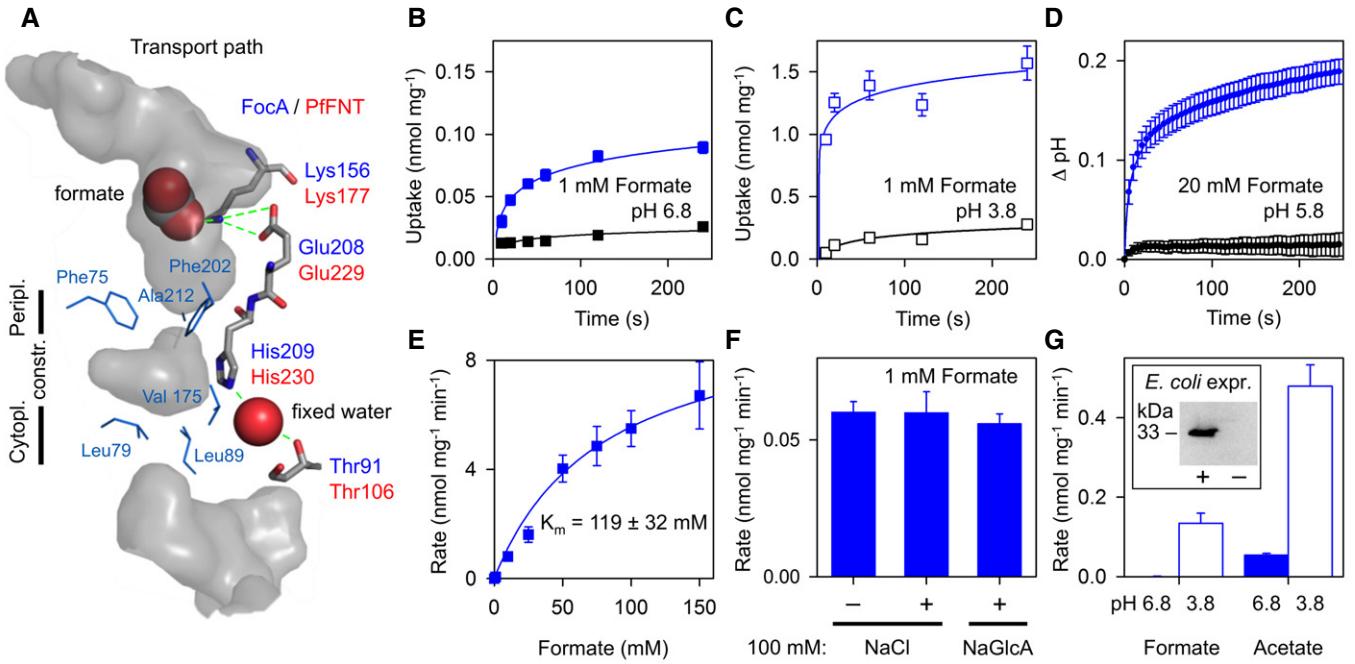

Figure 1. Formate/proton symport of FocA.

A Side view of the protomer chain A of the *Salmonella typhimurium* FocA (PDB# 3Q7K). The internal surface is shaded gray, and the amino acid residues forming the periplasmic and cytoplasmic constrictions are blue. Key residues of the transport path are shown as sticks (blue labels for FocA, red for PfFNT) and a fixed water molecule as sphere. In FocA, an invariant lysine (Lys156) forms a hydrogen bond (green, dashed line) to a formate substrate molecule.

B, C Uptake of ^{14}C-formate into yeast cells with (blue) or without expression of FocA (black) determined at pH 6.8 (B) and pH 3.8 (C). The data were obtained in a 1 mM inward gradient and normalized to 1 mg of dried yeast. Note the different scale of the ordinate by a factor of 10.

D Alkalization of the external, weakly buffered medium during uptake of formate into FocA-expressing yeast cells (blue); data of non-expressing control cells are shown in black.

E K_m determination from concentration-dependent formate uptake rates at pH 6.8 via FocA.

F Addition of 100 mM sodium chloride (NaCl) or sodium gluconate (NaGlcA) does not affect formate FocA transport.

G pH-dependent transport rates of FocA overexpressed in *E. coli*. The data were obtained in a 1 mM inward formate or acetate gradient and normalized to 1 mg dry weight of *E. coli* cells. The bars represent the difference in transport rates between FocA-expressing (+) and non-induced cells (–); see inserted Western blot.

Data information: Data were independently replicated: (B, C) four replicates; (D–G) three replicates. The error bars in all panels denote SEM.
Source data are available online for this figure.

In this study, using direct monitoring of radiolabeled substrate transport of bacterial FocA and protozoal PfFNT, we provide experimental evidence for a general selection and transport mechanism of the FNT family by direct one-step protonation of weak acid substrates. The previously described anion conductance of FocA is rapidly overwhelmed by proton motive force-driven transport of neutral formic acid at the provision of protons. We determined a decrease in substrate acidity by up to 3 pK_a units upon entering the hydrophobic FocA or PfFNT protein interior, and low activation energies of transport around 2 kcal mol^{-1}. From this, in conjunction with data from FocA mutants exhibiting altered electrostatic profiles and simulations of protein solvation in a water box, we conclude that FNTs electrostatically attract and funnel weak acid anions (A^-) into the hydrophobic transport path. The concomitant dielectric shift decreases substrate acidity facilitating protonation by the aqueous solvent and transport of the neutralized acid molecule (HA) across the hydrophobic constriction sites. At the core, this mechanism corresponds to that of Amt/Mep/Rh-type transporters for the weak bases ammonia and methylamine (Khademi *et al*, 2004), yet with opposite signs and thermodynamic consequences due to the required de-protonation of the positively charged base (BH^+) for neutralization (B). We conclude that weak acid and base neutralizing transporters, thus, represent functional counterparts of the same mechanistic class.

Results

FocA is a formate/proton symporter

We found before that the FocA homologue PfFNT from malaria parasites transports lactate in symport with protons (Wu *et al*, 2015). Accordingly, transport increased with the transmembrane proton gradient reaching maximal rates at pH conditions close to the substrate pK_a; concomitantly, the external assay solution alkalized indicating cotransport of protons (Wu *et al*, 2015). Several studies have addressed the pH-dependency of FocA (Lü *et al*, 2011, 2012a; Feng *et al*, 2012; Lv *et al*, 2013). One striking observation by an electrophysiology approach was a sharp switch in functionality at pH 5.8 below which formate transport apparently ceased.

However, the question remained controversial whether a pH-dependent gating mechanism shuts off transport altogether (Lü *et al*, 2011) or whether the transport mode changes abruptly to carrying protonated, electroneutral formic acid that goes unnoticed by electrodes (Lü *et al*, 2012a; Lv *et al*, 2013).

Adding ^{14}C-radiolabeled substrate to yeast suspensions expressing FocA allowed us to quantify total transport irrespective of the formate/formic acid protonation species (Fig 1B and C). In our setup, switching from a buffer of pH 6.8 to acidic pH 3.8, which corresponds to the substrate pK_a, resulted in a 20 times higher load of formate inside the cells after the 4-min assay time (0.06 versus 1.29 nmol mg^{-1}) and a 37 times higher initial transport rate (0.06 versus 2.23 nmol mg^{-1} min^{-1}). As found earlier with *Plasmodium* PfFNT (Wu *et al*, 2015), the medium alkalized during transport showing loss of protons most likely due to symport with formate (Fig 1D). The assay conditions of 20 mM formate at pH of 5.8 were chosen to lie outside the range of the formate-inherent buffer capacity (Wu *et al*, 2015), which is required to elicit a sufficient change in external pH. Saturation of transport occurred only at very high substrate concentrations (Fig 1E) yielding a v_{max} of 12.2 ± 1.8 nmol mg^{-1} min^{-1} and a low affinity, K_m, of 119 ± 32 mM. For FNT functionality, low anion affinity appears physiologically meaningful because it prevents FocA transport from being impeded by slowly passing, non-protonatable anions of strong acids, such as chloride (Lü *et al*, 2012a). Accordingly, addition to the assay buffer of chloride at a high, yet physiological concentration of 100 mM did not affect formate transport (Fig 1F). Impermeable gluconate was used at the same concentration as a control to exclude osmotic effects on FocA transport. Finally, we verified the pH-dependency of FocA transport in its physiological *Escherichia coli* environment. Again, formate transport increased when the external pH was switched from 6.8 to 3.8. The accumulation of transported substrate molecules appeared lower than in the yeast system, which we attribute to the activity of endogenous formate hydrogen lyases that rapidly convert formate to volatile carbon dioxide and dihydrogen. Hence, we additionally tested for transport of metabolically more stable acetate and yielded higher FocA transport rates despite a larger substrate size. Our results, thus, indicate that FocA transport does not cease at acidic pH due to a gating mechanism. To the contrary, FocA exhibits increased transport of protonated, neutralized substrate in response to the provision of protons.

A conserved lysine in the periplasmic vestibule attracts substrate anions

With the aim to locate and elucidate the FocA transport mechanism, we mutated key residues of the transport path and measured formate uptake rates at pH 6.8 and 3.8 (Fig 2A). A first set of mutations addressed the proposed central proton relay of FocA (Fig 1A; Lü *et al*, 2013). We replaced His209 with a similarly sized, polar asparagine (FocA H209N). Since the asparagine amide side chain is not protonatable, it lacks the possibility to act as a proton donor/acceptor. We further isosterically changed Thr91 to valine (FocA T91V) eliminating a stabilizing hydrogen bond to the fixed water molecule (red sphere in Fig 1A), whereas a third, conservative Thr91-to-serine exchange (FocA T91S) should retain the water in the FocA protein. The mutants were well expressed in yeast (Fig 2B). FocA H209N and T91V were non-functional, whereas

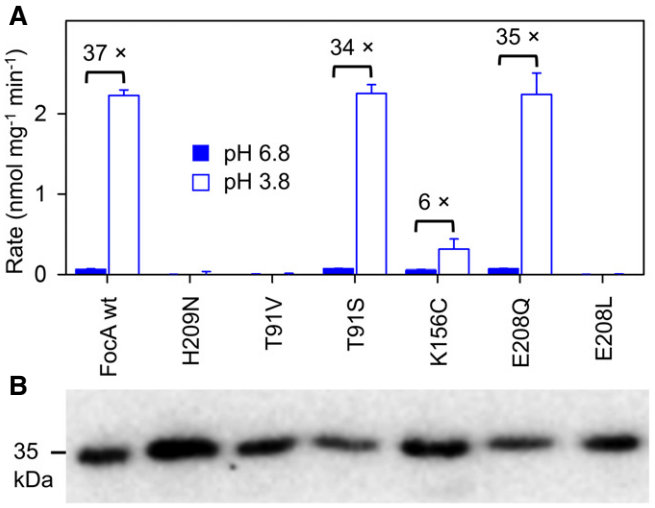

Figure 2. Functionality and pH-dependency of FocA mutants.

A Formate transport rates of FocA wild-type (wt) and mutants expressed in yeast at pH 6.8 (filled bars) as well as pH 3.8 (open bars). The fold increase in acidic medium is indicated above the bars for the functional FocA variants: wild-type, T91S, K156C, and E208Q, which all exhibited equal rates at pH 6.8. The error bars show SEM from three replications.

B Confirmation of expression by Western blot using an antibody against a C-terminally attached His-tag.

Source data are available online for this figure.

FocA T91S transport rates were equal to wild-type FocA (Fig 2A). Hence, both the imidazole side chain of His209 and the fixed water molecule seem indispensible for FocA transport (Hunger *et al*, 2014). The total loss of functionality, however, prevents further conclusions on their mechanistic contribution, which could be related to substrate protonation or purely structural.

It is energetically highly favorable when substrate neutralization occurs before passing the lipophilic FocA constrictions (Lv *et al*, 2013). Therefore, it is questionable whether the central His209 is suited for the protonation of formate, because the imidazole side chain is positioned in the hydrophobic space between the lipophilic constrictions (Fig 1A). Lys156, however, is striking due to its location just above the periplasmic constriction close to the bulk solvent; in fact, some protomers of FocA crystals grown in formate containing buffer were found to carry formate in hydrogen bond distance to Lys156 (Fig 1A; Lü *et al*, 2011). Lys156 is even more conserved than the central histidine for which incidental substitutions by asparagine can be found in the databases (e.g., *Entamoeba histolytica* FNT; Marchetti *et al*, 2015). Further, a second conserved lysine is typically found to be placed symmetrically in the cytoplasmic transporter vestibule, which complies with observations of bidirectional transport of FNT proteins (Czyzewski & Wang, 2012; Wu *et al*, 2015). In a new set of FocA mutants, we first changed the external facing, positively charged Lys156 to a neutral cysteine (FocA K156C). FocA K156C was well expressed and functional (Fig 2A and B). In fact, under standard assay conditions at pH 6.8, the transport rates of FocA wild-type and K156C were equal within experimental precision (0.05 nmol mg^{-1} min^{-1}; Fig 2A). The increase in transport at pH 3.8, however, was only sixfold, that is, one-sixth compared to wild-type FocA (Fig 2A).

Two additional FocA mutants carrying a hydrophobic residue at the lysine position, K156A and K156M, behaved similarly (Fig EV1). To further evaluate the role of Lys156 on pH-dependent transport of FocA, we generated mutants of the neighboring, buried Glu208 because its side chain carboxyl group resides in hydrogen bond distance to the ε-amino group of Lys156 forming a pair of electrostatic interaction (Fig 1A). We replaced Glu208 by glutamine to eliminate the negative charge but to keep the fixating hydrogen bonds (FocA E208Q), and by a similarly sized, non-interacting leucine (FocA E208L). The expression levels of both mutants were similar to wild-type FocA (Fig 2B), yet only FocA E208Q was functional (Fig 2A) suggesting that the hydrogen bonds to Lys156 have a crucial structural function.

To assess the electrostatic role of the Lys156 site on FocA substrate attraction and transport, we calculated the Poisson–Boltzmann electrostatic potential (Baker *et al*, 2001) for FocA E208Q, wild-type, and K156C (Fig 3A). As expected, the positive potential around Lys156 is increased in FocA E208Q due to the lack of a negative countercharge at the former glutamate position, whereas FocA K156C is strongly negative because the charge at E208 fully emanates into the hydrophobic vestibule.

The changes in electrostatics had functional consequences as we noticed by determining pH-dependent transport profiles and substrate affinity. The pH curve obtained with FocA wild-type (Fig 3B) exhibited the same shape as monitored before with PfFNT (Wu *et al*, 2015); that is, transport increased toward acidic pH and was maximal around the pK_a of formate. We further confirmed that FocA transport is proton motive force-driven, because formate uptake ceased upon disruption of the transmembrane proton gradient by protonophores (Fig 3B, open symbols). Transport via the FocA K156C mutant appeared largely independent of the buffer pH (Fig 3C). The small rise in transport at pH 3.8 coincides with the disappearance of the anionic formate species from the buffer and the appearance of the neutral formic acid species, respectively, according to the chemical protonation equilibrium (dotted line in Fig 3C). This implies that the neutral formic acid form can enter the hydrophobic transport path fairly unhindered, whereas the formate anion is actively repelled by the negative electrostatics of FocA K156C. FocA E208Q produced a highly similar transport profile to wild-type FocA (Fig 3B and D) despite an elevated positive electrostatic field at the entrance site, which should increase attraction of substrate anions to the transporter. Indeed, substrate affinity to FocA E208Q (Fig 3E) was about twice as high as to wild-type FocA (K_m = 51 ± 20 mM). This effect is leveled out, however, by reduced maximal transport rates by a similar factor (v_{max} = 7.7 ± 1.2 nmol mg^{-1} min^{-1}) leading to the observed wild-type-like transport. Substrate affinity to FocA K156C was too weak for experimental determination of K_m.

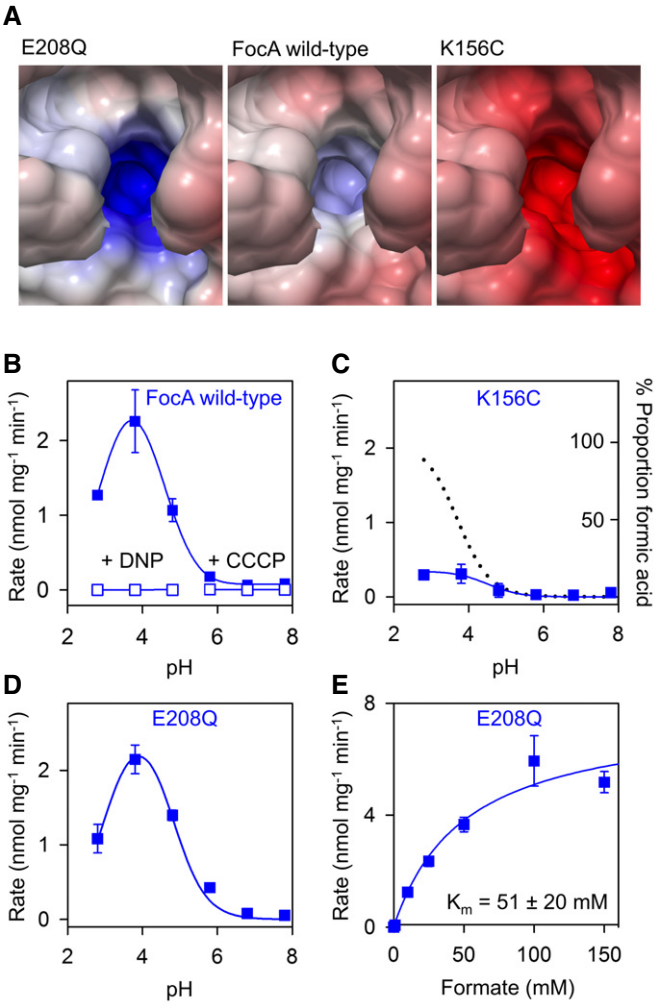

Figure 3. Electrostatic effect of Lys156 of the periplasmic vestibule on FocA transport.

A Poisson–Boltzmann electrostatic potential of FocA wild-type (middle panel) in comparison to the FocA mutants E208Q (left) and K156C (right).

B–D Profiles of pH-dependent formate transport of FocA wild-type (B), FocA K156C (C), and FocA E208Q (D) in yeast. Formate transport ceased upon treatment with protonophores 2,4-dinitrophenol (DNP) and carbonyl cyanide m-chlorophenylhydrazone (CCCP; open symbols in B). The dotted line in (C) depicts the proportion of protonated, neutral formic acid in the formate solution depending on the protonation equilibrium.

E K_m determination of FocA E208Q.

Data information: All data points in panels (B–E) are from independent replicates: (B, C) four replicates; (D, E) three replicates. Error bars denote SEM.

Substrate acidity is decreased in the hydrophobic FNT transport path

The pH-dependent transport profile of FocA is bell-shaped and closely resembles the earlier established pH profile of lactate transport via the malaria parasite's PfFNT (Wu *et al*, 2015). If transport via FocA and PfFNT would be determined by a single pK_a, for example, that of the weak acid substrate in buffer solution, then the respective curve shape would be sigmoidal (see Fig 3C). Bell-shaped pH effect curves, however, typically derive from dependency of two pK_a values.

We figured that the substrate itself may exhibit two different pK_a values resulting from a shift to lower acidity when moving from the aqueous solvent (pK_{a1}, known standard parameter) into the hydrophobic FNT transport path (pK_{a2}, unknown). A hydrophobic environment is less permissive to dissociation of a neutral acid molecule into the acid anion and a proton to prevent the appearance of non-compensated charges that are energetically unfavorable. The pH-dependent fractions of substrate anion and neutral substrate in

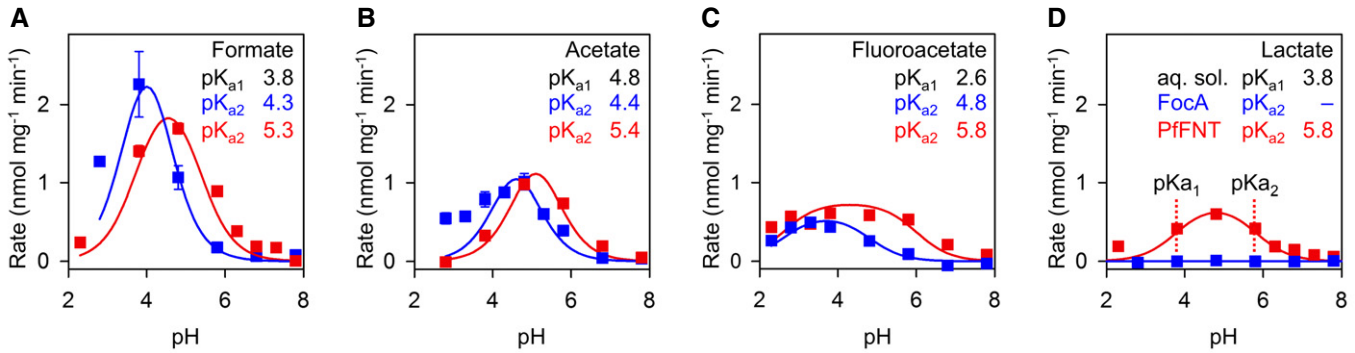

Figure 4. Substrate acidity in the periplasmic FNT vestibule.

A–D Measurements of pH-dependent transport rates of FocA (blue squares) and PfFNT (red squares) for formate (A), acetate (B), fluoroacetate (C), and L-lactate (D). The data points were obtained from four independent yeast transformations (± SEM). Fitting to two combined Henderson–Hasselbalch equations (lines; see text for details) yielded the apparent pK_{a2} of the substrate in the FNT vestibule as denoted by the inflection points of the bell-shaped curves (see panel for L-lactate).

the aqueous solvent and in the hydrophobic FNT vestibule are given by two combined Henderson–Hasselbalch equations (Gordon-Beresford *et al*, 1996):

$$\text{Rate} \propto \frac{c_1}{10^{pK_{a1}-pH}+1} \cdot \left(c_2 - \frac{c_2}{10^{pK_{a2}-pH}+1}\right)$$

with c_1 and c_2 being the concentrations of substrate and FNT, respectively. The pK_{a1} and pK_{a2} values define the inflection points of the resulting bell-shaped curve, and the pH condition for the maximal transport rate is given by the mean of both pK_a values.

We titrated the pK_{a2} values of substrates with different acidity by measuring transport rates with FocA and PfFNT (Fig 4, symbols) and fitting of the data using the equation above (Fig 4, lines). The curves exhibit expected differences between FocA and PfFNT with respect to substrate selection by size (see lactate curves in Fig 4D) but also reveal shifts in the pH optima. The obtained pK_{a2} values appeared independent of substrate acidity in the aqueous solvent but roughly correlated with substrate size (Table 1). For FocA, we obtained a range from pK_{a2} = 4.3 (formate) via 4.4 (acetate) to 4.8 (fluoroacetate). With PfFNT, we found a generally larger shift of pK_{a2} by one logarithmic unit to 5.3 (formate), 5.4 (acetate), and 5.8 (fluoroacetate, lactate). As a consequence, transport rates of PfFNT at close to neutral pH, that is, at low proton motive force, are higher than those of FocA, the latter requiring steeper gradients for high-capacity transport. It is further remarkable that more voluminous substrates yielded higher apparent pK_{a2} values meaning that the transport hindrance by size is partially compensated for by increased protonation efficiency. This effect may be particularly relevant for the physiological function of PfFNT as a lactate/proton symporter in malaria parasites.

Toward an FNT transport model

Our data so far suggest an FNT transport mechanism in which weak acid anions are electrostatically funneled into a hydrophobic transport path where protonation occurs, that is, neutralization, due to dielectric decrease in substrate acidity, eventually enabling passage through the hydrophobic FNT constrictions.

A mechanism according to this model has energetic and kinetic consequences, which can be experimentally addressed. A downshift in substrate pK_a representing the major component of FNT selectivity and transport would call for rather low activation energies of transport (E_a). According to $\Delta G^0 = 2.303\ R\ T\ \Delta pK_a$ (R, gas constant; T, absolute temperature; Sarmini & Kenndler, 1999), the observed shift of 1–2 pK_a units translates into free energies of 5.7–11.4 kJ mol^{-1} (1.4–2.7 kcal mol^{-1}). We determined activation energies for the transport of formate in exactly this range with $E_{a,\ FocA}$ = 2.2 ± 0.5 kcal mol^{-1} and $E_{a,\ PfFNT}$ = 1.5 ± 0.4 kcal mol^{-1} (Fig 5A).

Another central question would concern the mechanism of proton transfer to the substrate anion. To decide whether substrate

Table 1. Properties of FNT substrates.

	Substrate		FocA		PfFNT	
	Vol. (Å^3)	pK_{a1}	Max. transp. rate (nmol mg^{-1} min^{-1})	pK_{a2}	Max. transp. rate (nmol mg^{-1} min^{-1})	pK_{a2}
Formate	36.8	3.8	2.5	4.3 ± 0.2	2.0	5.3 ± 0.2
Acetate	53.5	4.8	1.1	4.4 ± 0.2	1.7	5.4 ± 0.3
Fluoroacetate	58.5	2.6	0.5	4.8 ± 0.5	0.7	5.8 ± 0.3
L-lactate	79.1	3.8	—	—	0.6	5.8 ± 0.4

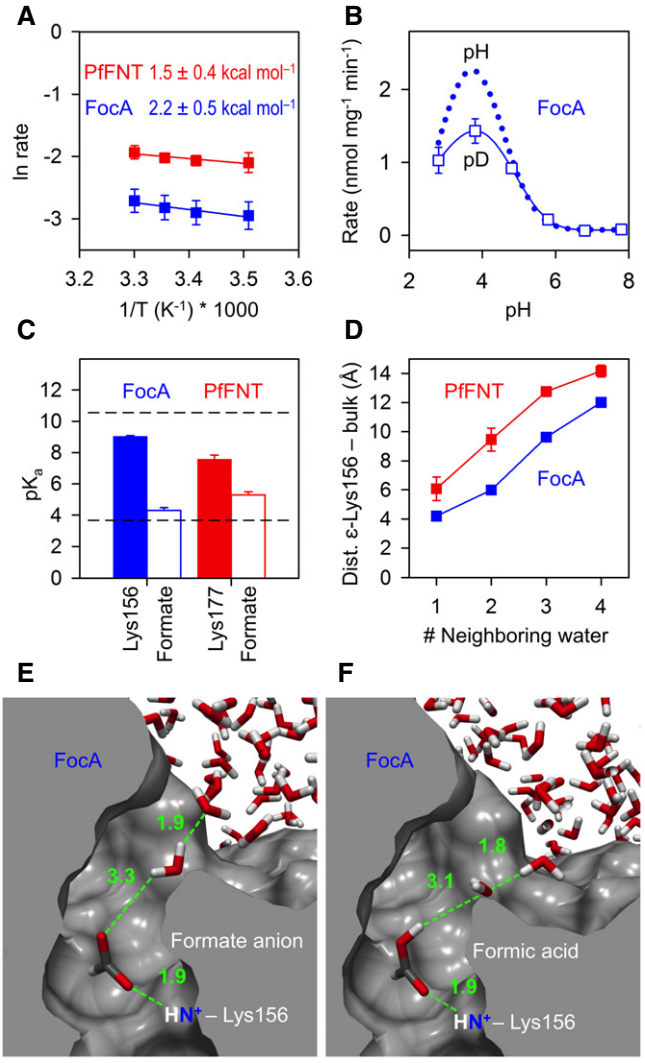

Figure 5. Single-step protonation of formate in the process of isolation from the bulk solvent.

A Low activation energy of formate transport via FocA (blue) and PfFNT (red) in yeast. SEM is derived from three experiments.

B Heavy water effect, D_2O, on the maximal formate transport rate in yeast. The reduction by 35% indicates a single proton/deuteron transfer event; the dotted line indicates rates of FocA wild-type taken from Fig 3B. SEM is derived from four experiments.

C Dielectric shift in pK_a of the conserved lysine (Lys156 in FocA, blue; Lys177 in PfFNT, red; filled bars) and the formate substrate (open bars) in the periplasmic FNT vestibule. The dashed lines indicate undisturbed pK_a values of lysine (10.5) and formate (3.8) in aqueous solution. The error bars denote SEM from calculations using the five individual transport units in the FNT pentamer.

D Calculation of the residue depth with respect to the bulk solvent. Shown is the distance of the ε-amino group of Lys156 in FocA (blue) and Lys177 in PfFNT (red) to water clusters of the bulk solution. The number of neighboring water molecules indicates how many water molecules are in hydrogen bond distance to the water closest to Lys156 or Lys177. The error bars denote SEM from calculations using the five individual transport units in the FNT pentamer.

E, F Solvation simulation of FocA with a formate anion (E) and neutral formic acid (F) in the periplasmic vestibule. The snapshots show the situations of closest approximation of bulk water to the ε-amino group of Lys156. Distance measurements along the green dashed lines are in angstrom.

neutralization is by direct single-step protonation or by the proposed multi-step proton relay involving the central histidine, we made use of the reduced deuteron mobility of heavy water, D_2O. Since deuterons have twice the mass of a proton and the strength of a bond is increased, their mobility is reduced by about 30% (DeCoursey & Cherny, 1997; Beitz *et al*, 2006). This way, a mechanism involving a single deuteron transfer should be slightly impeded by about one-third, whereas a multi-step transfer process would appear greatly impaired. We prepared formate assay solutions from heavy water, D_2O, in a range of pD 2.8–7.8 and found a decrease in the maximal transport rate by 35% (Fig 5B), which is indicative of a single proton transfer mechanism rather than a relay. This conclusion is further supported by the very low activation energy of FNT transport, which corresponds to the energetic cost of breaking a single charged hydrogen bond (Fersht *et al*, 1985).

With the central histidine rendering an unlikely site for proton transfer, we aimed at identifying an alternative proton donor. Inspection of the path-lining amino acid residues of the FocA transporter left only one ionizable residue, that is, Lys156, located in the periplasmic vestibule (Fig 1A). Being a strong base, however, this lysine would require a dramatic disturbance in pK_a from 10.5 in aqueous solution by 5–6 log units to meet the pK_{a2} of formate in the transporter vestibule (pK_{a2} = 4.3 in FocA, and 5.3 in PfFNT; Fig 4). We, thus, calculated the pK_a of Lys156 (FocA; PDB# 3Q7K) and the corresponding Lys177 (PfFNT model; Wu *et al*, 2015) using the residue depth approach (Chakravarty & Varadarajan, 1999) that is based on distance measurements of each atom in a protein to the bulk solvent by repeated solvation cycles (Fig 5C). We obtained reduced pK_a values of 9.0 ± 0.1 for Lys156 of FocA and 7.6 ± 0.3 for Lys177 of PfFNT, respectively (Fig 5C). However, the remaining gap to a formate in the vestibule in the range of 3–4 pK_a units appears too large to allow proton transfer and, thus, probably excludes Lys156 of FocA and Lys177 of PfFNT, respectively, as a proton donor.

The residue depth calculation further revealed a distance much greater than a hydrogen bond of 4.2 Å between the bulk water and the ε-amino group of Lys156 in FocA and even 6.1 Å to Lys177 in PfFNT (Fig 5D) indicating a somewhat more hydrophobic environment for the latter. This led us to additionally simulate solvation of FocA with both a negatively charged formate ion and a neutral formic acid molecule placed next to Lys156. The snapshots in Fig 5E and F depict the situations of closest approach of a bulk water molecule to the anionic and neutral substrates. In either case, the distance between substrate and water was > 3 Å meaning that the substrate will become isolated from the water bulk when approaching the lysine. As a consequence, we conclude that the substrate-neutralizing proton is derived from the bulk water. It will be transferred at a specific point of substrate approximation to the lysine in the hydrophobic vestibule when the substrate acidity has been sufficiently lowered by the dielectric environment. As a neutral molecule, it can fully enter and pass the hydrophobic FNT transport path.

Discussion

Our experimental data provide insight into FNT transport with regard to gating, proton transfer, and anion transport versus anion/proton symport. Earlier studies suggested a pH-gating mechanism of

FocA (Lü *et al*, 2011). It was concluded from crystal data that the N-terminal domain assumes a helical structure that would occlude the pore in the acidic range, whereas an unstructured N-terminus at neutral pH would represent the open conformation. Yet, we found a steady increase in FocA transport rates from neutral to acidic assay conditions, that is, a permanently open conformation. This is in agreement with a recent molecular dynamics simulation study (Lv *et al*, 2013). It showed that, independent of the conformation, the FocA N-terminus cannot sufficiently narrow the pore entry to prevent formate from passing (Lv *et al*, 2013). Apparently, the loss of electrogenic anion transport as determined in an electrophysiology setup was initially misinterpreted as closure of the transporter (Lü *et al*, 2011, 2012a). Electrogenic formate transport occurs at close to neutral pH conditions and trails off when the pH is shifted toward acidic buffer conditions (Lü *et al*, 2012a). We found that with increasing proton motive force toward acidic pH, the transport of protonated, neutral substrate rapidly becomes predominant; the onset of electroneutral anion/proton symport depends on the FNT isoform as seen by comparison of the PfFNT and FocA pH profiles. Currently, it is not possible to quantify the fractions of charged and uncharged substrate transport due to incompatible assay systems. However, in our setup, destruction of the proton gradient by protonophores decreased transport rates to the background noise level even at neutral pH. This suggests that besides some anion leakage as observed by electrophysiology, anion/proton symport is the major transport mechanism of FNTs. Proton cotransport is meaningful on the physiological level as well, because the bacterial formate hydrogen lyase reaction depends on both the formate anion, $HCOO^-$, and a proton, H^+, for the generation of CO_2 and H_2 (Sawers, 2005).

We propose a general FNT anion/proton symport mechanism by three steps: (i) electrostatic attraction of the substrate anion to the FNT, (ii) concomitant dielectric shift of substrate acidity leading to neutralization by proton transfer from the bulk solvent, and (iii) passage of the neutral substrate via the lipophilic constrictions. This model is complementary to that of ammonium transporters, for example, AmtB, which are thought to abstract a proton from the charged ammonium cation, NH_4^+, for neutralization and subsequent passage of ammonia, NH_3, via a hydrophobic transport channel (Khademi *et al*, 2004).

The FNT transport path emanates a positive electrostatic field due to the helix dipole moment at the so-called L2 and L5 loop regions (Wang *et al*, 2009), a possibly protonated central histidine (Lü *et al*, 2013; Lv *et al*, 2013), and the invariant lysine in the FNT periplasmic vestibule. Formate molecules in FocA crystals at low, that is, physiological, substrate concentration have been found next to the lysine (Wang *et al*, 2009; Lü *et al*, 2011) despite a very low apparent affinity (Lü *et al*, 2012a). Low, channel-like substrate affinities clearly distinguish FNTs from classical transporters, for example, of the alternating access type, which can be seen as a protection against inhibition (Song *et al*, 2016) by abundant anions with slow transport rates, such as chloride (Lü *et al*, 2012a). The proton motive force dependency of FNTs, however, is a typical feature of secondary transporters.

Proton transfer to the transported substrate critically depends on the respective proton affinities. It is remarkable that even the strongly acidic fluoroacetate with a pK_a of 2.6 is transported in a pH-dependent fashion. Despite a 100-fold higher acidity, the maximal transport rate is still 45% of the similarly sized acetate (Table 1). But what is the source of the transport-enabling proton? There are examples showing dramatic pK_a disturbances of lysine when the residue is positioned in a highly lipophilic protein environment (Ho *et al*, 2009; Isom *et al*, 2011; Balashov *et al*, 2013). However, pK_a calculations show that the hydrophobic environment of the FocA vestibule does not shift the basicity of lysine enough to become a substrate-protonating acid. Instead, our solvation simulations and distance measurements suggest protonation of the substrate by the aqueous bulk upon entering the hydrophobic vestibule. In this regard, it is noteworthy that larger substrates led to higher pK_{a2} values, that is, an increased tendency of the substrate to become protonated, which possibly derives from better shielding from the bulk rendering the vestibule more hydrophobic.

The Born equation on solvation free energy, ΔG^0, provides a simple way to relate a shift in pK_a to the dielectric constants of a solvent continuum, ε_s, and water, ε_w (Born, 1920; Sarmini & Kenndler, 1999):

$$\Delta G^o = \left(N z^2 e^2\right)/2r \times \left(1/\varepsilon_s - 1/\varepsilon_w\right)$$

with N being the Avogadro constant, z the charge number, e the elemental charge, r the ion radius in angstrom (≈ 2 Å for a carboxyl group), R the gas constant, and T the absolute temperature. The observed ΔpK_a of formate in the FocA and PfFNT vestibules is 1 ± 0.5; that for fluoroacetate is 2.3 ± 0.5. This translates into alterations of the dielectric constants from the water bulk of $\varepsilon_w = 78.3$ to the FocA or PfFNT vestibules of $\varepsilon_s = 34.3$ for formate and $\varepsilon_s = 19.8$ for fluoroacetate, respectively. A hydrophobic protein core is characterized by dielectric constants in the range of 2–10 (Mertz & Krishtalik, 2000). The obtained dielectric constants of the FNT vestibules, thus, signify that a substrate encounters a significant yet still moderate increase in hydrophobicity during the transition into the FNT transport path. In conjunction with the observed electrostatic attraction yet low substrate affinity, the dielectric and electrostatic properties of the vestibule seem to be carefully balanced to achieve efficient transport at minimal energetic cost.

FNTs and ammonium transporters (Khademi *et al*, 2004) exhibit the same principle for substrate selectivity by proton transfer and subsequent transport of the neutral substrate species via a lipophilic transport path. Due to the partly opposite characteristics of weak acid and base substrate molecules, however, certain aspects regarding electrostatics, thermodynamics, and pH-dependency of transport are quite different. First, weak acids and bases are oppositely charged at physiological pH. Therefore, FNTs attract substrates by a positive electrostatic field as laid out above, whereas the electrostatic field at the ammonium transporter entry is negative due to the indirect effect of a conserved aspartate that orients protein backbone carbonyls toward the transport path (Khademi *et al*, 2004; Fig EV2, Asp160). Second, protonation of a weak acid anion, $A^- + H^+ \rightarrow HA$, eliminates by combination two charges from the solvent, whereas neutralization of a protonated base, $BH^+ \rightarrow B + H^+$, leaves the number of charged molecules unaltered. As a consequence, acid anion neutralization is powered by a substantial increase in entropy by freeing water molecules from the ion hydration shells, whereas dissociation of the protonated base requires an enthalpic contribution. Nevertheless, the activation energy of the *E. coli* ammonium transporter, AmtB, was determined to 1.6 kcal mol^{-1}, that is, equally low as our data on formate transport

of FocA and PfFNT (Javelle *et al*, 2005). Third, due to the protonation step, transport of weak acid anions benefits from the proton motive force leading to higher transport rates in the acidic range, whereas transport of weak bases does not. Ammonium transporters, thus, function largely independent of the pH (Khademi *et al*, 2004). Still, yeast cells, for instance, need to take up ammonium as a vital nitrogen source even at very low concentrations in the environment (Khademi *et al*, 2004). As a consequence, ammonium transporters typically exhibit high substrate affinity in the micromolar range (Neuhäuser *et al*, 2014); substrate affinity of FocA, in turn, is low.

Despite these substrate-derived differences, the overall layout of the individual transport units in pentameric FNTs and trimeric ammonium transporters is quite similar. In both cases, the central transport path of each promoter is a non-flexible, narrow, and hydrophobic tube holding one (FNTs; Fig 1A) or two histidines (ammonium transporters; Fig EV2). The histidines in ammonium transporters are assumed be uncharged (Javelle *et al*, 2006); we cannot conclude on the debated protonation state of His209 in FocA by this study. Yet, due to the observed low positive activation energy that matches earlier molecular dynamic simulations of FocA with a neutral His209 (Lv *et al*, 2013), we prefer to think of the histidine as non-protonated. In both protein families, lipophilic constriction sites occlude the central path (see Fig 1A for FNTs); ammonium transporters contain a double phenylalanine gate (Fig EV2). The FocA constrictions allow for substrate passage by channel-opening flickering of the lipophilic residue side chains on a very fast timescale as found by single channel recordings (Lü *et al*, 2012a). The phenylalanine gate of ammonium transporters is thought to act similarly (Javelle *et al*, 2008). Finally, and key to the transport mechanism, funnel-like vestibules connect the hydrophobic transport paths of FNTs and ammonium transporters to the aqueous bulk and facilitate substrate neutralization by proton transfer due to dielectric shift of substrate acidity. Together, it seems justified to join weak acid and base neutralizing transporters into one mechanistic class.

Materials and Methods

Expression plasmids, mutation, transformation, and culture

Codon-optimized PfFNT in the yeast expression vector pDR196 has been described (Wu *et al*, 2015). EcFocA (Wang *et al*, 2009) was amplified from genomic *E. coli* DNA and cloned in pDR196 via SpeI/XhoI, to additionally encode an N-terminal hemagglutinin epitope and a C-terminal His_{10} tag (35 kDa). For expression in *E. coli*, EcFocA was cloned into pET21 (Novagen) via BamHI/HindIII with a C-terminal His_6 tag (33 kDa). Point mutations were introduced according to the QuikChange protocol (Stratagene) using primers with respective nucleotide exchanges (Life Technologies; the primers are listed in Table EV1). All constructs were sequenced for verification. W303-1A jen1Δ ady2Δ (MATa, can1-100, ade2-1oc, his3-11-15, leu2-3,-112, trp1-1-1, ura3-1, jen1::kanMX4, ady2::hphMX4) yeast cells, kindly provided by M. Casal, were transformed using the lithium acetate/single stranded carrier DNA/polyethylene glycol procedure (Gietz *et al*, 1995). Transformed yeast was grown at 30°C in selective media (SD) without uracil and containing adenine, histidine, leucine, tryptophan, and 2 % (wt/vol) glucose.

Yeast membrane protein preparation and Western blot

Yeast cells from 100 ml culture were collected (1,000 *g*, 5 min) at an OD_{600} of 1 and washed with 25 ml water and 10 ml extraction buffer (5 mM EDTA, 25 mM Tris, pH 7.5), pelleted, and resuspended in 0.5 ml extraction buffer. Cells were disrupted by adding 0.5 g acid-washed glass beads (Sigma-Aldrich, Ø 0.5 mm) and ten cycles of vortexing and cooling of 30 s each. The supernatant was centrifuged at 100,000 *g* for 40 min, and the obtained membrane protein pellet was resuspended in 0.1 ml 100 mM phosphate buffer, pH 8.0, with 50 mM NaCl. Proteins were separated by SDS–PAGE, blotted on PVDF membranes (Hybond-P; Amersham Biosciences), and probed with a monoclonal anti-penta-His antibody (Qiagen). Detection was done using a horseradish peroxidase-conjugated secondary antibody (Jackson ImmunoResearch) and the ECL Plus Western blotting detection system (GE Healthcare) and documented with a Lumi-Imager F1 (Roche).

Direct transport assays using radiolabeled substrates

Assays were done as described earlier (Wu *et al*, 2015). Briefly, for standard assay conditions, yeast was suspended in 50 mM HEPES/Tris, pH 6.8, to an OD_{600} of 50 (± 10%), and kept on ice. Other pH conditions were established using 50 mM HEPES/Tris (pH 6.8–7.8), 50 mM MES/Tris (pH 5.8), and 50 mM citric acid/Tris (pH 2.8–4.8). The assays were carried out with at least three replicates of each data point at 18°C in 1.5-ml reaction tubes containing 80 µl aliquots of yeast suspension. Transport was initiated by adding 20 µl of substrate solution to yield a final concentration of 1 mM substrate and 0.04 µCi radiolabeled [1-^{14}C]-substrate (formate, acetate, fluoroacetate, or L-lactate). The reaction was stopped by abrupt dilution with 1 ml ice-cold water, rapid transfer onto a vacuum filtration unit fitted with a GF/C filter membrane (Whatman), and washing with 7 ml water. The filter membranes were transferred to scintillation vials containing 3 ml of scintillation fluid (Quicksafe A; Zinsser Analytic) and analyzed using a Packard TriCarb liquid scintillation counter (Perkin Elmer Inc.). Proton decoupling was achieved by addition of 1 mM 2,4-dinitrophenol (DNP, from a 100 mM stock in 70% ethanol; Sigma-Aldrich) or 50 mM carbonyl cyanide-3-chlorophenylhydrazone (CCCP, from a 10 mM stock solution in 70% ethanol; Sigma-Aldrich) to the cell suspension 15–20 min before the experiment. The data range was split according to the protonophores' pK_a (DNP, pK_a 4.0, pH range 2.8–4.8; CCCP, pK_a 6.09, pH 5.8–8.8; McLaughlin & Dilger, 1980). For comparative measurements in H_2O versus D_2O (99.9% purity; Roth), cells were collected and resuspended in McIlvaine buffer (McIlvaine, 1921) with defined pH/pD by adding solid citric acid and disodium phosphate.

Recordings of external pH during formate uptake

Yeast cells were grown to an OD_{600} of 1 (mid-log phase), collected by centrifugation at 2,000 *g* for 5 min at 4°C, and washed twice with deionized water. Cells were resuspended to an OD_{600} of 60 in weakly buffered incubation solution (4 mM MES, pH 5.8, 0.5% deoxy-D-glucose). 1 ml of the cell suspension was diluted into 7 ml using deionized water. Uptake was initiated by addition of 20 mM sodium formate from a 1 M stock solution prepared in deionized water. The pH of the external buffer was recorded at intervals of 5 s

by using a SenTix950 pH electrode connected to a Multi9310 pH meter (WTW GmbH, Germany). All measurements were carried out at room temperature.

FocA expression in *E. coli*

Transformed BL21 (DE3) pRep4 [F^- *omp*T hsdSB(rB^-, mB^-) *gal dcm* (DE3) pRep4 (neo)] cells were grown aerobically at 37°C to an OD_{600} of 0.6 in LB medium (Gibco) supplemented with ampicillin (100 μg ml^{-1}) and kanamycin (40 μg ml^{-1}). FocA expression from pET21 was induced by addition of 0.1 mg ml^{-1} isopropyl-β-D-thiogalactopyranoside (IPTG) for 3 h. Cells were collected at 4000 *g* for 10 min and resuspended to an OD_{600} of 10 (± 5%) in 72 mM NaCl, 0.2% glucose, and 50 mM HEPES, pH 6.8 or 3.8, respectively. Transport assays were done as described above with 0.1 μCi radiolabeled [1-^{14}C]-formate or acetate and 0.45-μm nylon filter membranes (Whatman). For the Western blot, resuspended cell pellets were disrupted by sonication.

Calculations of electrostatic potential, pK_a, and solvation

All calculations were done using the PDB structure file 3Q7K for FocA and a PfFNT model (Wu *et al*, 2015) based on 3Q7K. For Poisson–Boltzmann electrostatics, the APBS tool (Baker *et al*, 2001) was used from within the Chimera software (Pettersen *et al*, 2004). Predictions of pK_a were done via residue depth in a water box using the SPC216 water model (Chakravarty & Varadarajan, 1999; Tan *et al*, 2013). For solvation cycles of FocA with bound formate and formic acid, the protein structure was repeatedly rotated and translated in an SPC/Fw water box using amber tools (Case *et al*, 2016) from within the Chimera software (Pettersen *et al*, 2004).

Expanded View for this article is available online.

Acknowledgements

We thank B. Henke, A. Fuchs, and S. Häuer for technical assistance as well as M. Casal for providing the *jen1*Δ *ady2*Δ yeast strain, and J. Holm-Bertelsen for the pET21-FocA construct. G. Sawers and D. Hunger are acknowledged for help with the *E. coli* system. Molecular graphics and analyses were performed with the PyMOL Molecular Graphics System, version 1.7 (Schrödinger, LLC), and the UCSF Chimera package. Chimera is developed by the Resource for Biocomputing, Visualization, and Informatics at the University of California, San Francisco (supported by NIGMS P41-GM103311). This work was funded by the Deutsche Forschungsgemeinschaft (Be2253/6-3).

Author contributions

MW performed the experiments and analyzed the data; EB designed the study, conducted simulations, analyzed the data, and wrote the manuscript.

Conflict of interest

The authors declare that they have no conflict of interest.

References

Baker NA, Sept D, Joseph S, Holst MJ, McCammon JA (2001) Electrostatics of nanosystems: application to microtubules and the ribosome. *Proc Natl Acad Sci USA* 98: 10037 – 10041

Balashov SP, Petrovskaya LE, Imasheva ES, Lukashev EP, Dioumaev AK, Wang JM, Sychev SV, Dolgikh DA, Rubin AB, Kirpichnikov MP, Lanyi JK (2013) Breaking the carboxyl rule: lysine 96 facilitates reprotonation of the Schiff base in the photocycle of a retinal protein from *Exiguobacterium sibiricum*. *J Biol Chem* 288: 21254 – 21265

Beitz E, Wu B, Holm LM, Schultz JE, Zeuthen T (2006) Point mutations in the aromatic/arginine region in aquaporin 1 allow passage of urea, glycerol, ammonia and protons. *Proc Natl Acad Sci USA* 103: 269 – 274

Born M (1920) Volumen und Hydratationswärme der Ionen. *Z Phys* 1: 45 – 48

Case DA, Betz RM, Cerutti DS, Cheatham TE III, Darden TA, Duke RE, Giese TJ, Gohlke H, Goetz AW, Homeyer N, Izadi S, Janowski P, Kaus J, Kovalenko A, Lee TS, LeGrand S, Li P, Lin C, Luchko L, Luo R *et al* (2016), AMBER 2016, University of California, San Francisco

Chakravarty S, Varadarajan R (1999) Residue depth: a novel parameter for the analysis of protein structure and stability. *Structure* 7: 723 – 732

Clegg S, Yu F, Griffiths L, Cole JA (2012) The roles of the polytopic membrane proteins NarK, NarU and NirC in *Escherichia coli* K-12: two nitrate and three nitrite transporters. *Mol Microbiol* 44: 143 – 155

Czyzewski BK, Wang DN (2012) Identification and characterization of a bacterial hydrosulphide ion channel. *Nature* 483: 494 – 497

Das P, Lahiri A, Lahiri A, Chakravortty D (2009) Novel role of the nitrite transporter NirC in *Salmonella* pathogenesis: SPI2-dependent suppression of inducible nitric oxide synthase in activated macrophages. *Microbiology* 155: 2476 – 2489

DeCoursey TE, Cherny VV (1997) Deuterium isotope effects on permeation and gating of proton channels in rat alveolar epithelium. *J Gen Physiol* 109: 415 – 434

Feng Z, Hou T, Li Y (2012) Concerted movement in pH-dependent gating of FocA from molecular dynamics simulations. *J Chem Inf Model* 52: 2119 – 2131

Fersht AR, Shi JP, Knill-Jones J, Lowe DM, Wilkinson AJ, Blow DM, Brick P, Carter P, Waye MM, Winter G (1985) Hydrogen bonding and biological specificity analysed by protein engineering. *Nature* 314: 235 – 238

Gietz RD, Schiestl RH, Willems AR, Woods RA (1995) Studies on the transformation of intact yeast cells by the LiAc/SS-DNA/PEG procedure. *Yeast* 11: 355 – 360

Gordon-Beresford RM, van Belle D, Giraldo J, Wodak SJ (1996) Effect of nucleotide substrate binding on the pK_a of catalytic residues in barnase. *Proteins* 25: 180 – 194

Ho MC, Ménétret JF, Tsuruta H, Allen KN (2009) The origin of the electrostatic perturbation in acetoacetate decarboxylase. *Nature* 459: 393 – 397

Hunger D, Doberenz C, Sawers RG (2014) Identification of key residues in the formate channel FocA that control import and export of formate. *Biol Chem* 395: 813 – 825

Isom DG, Castañeda CA, Cannon BR, García-Moreno B (2011) Large shifts in pK_a values of lysine residues buried inside a protein. *Proc Natl Acad Sci USA* 108: 5260 – 5265

Javelle A, Thomas G, Marini AM, Krämer R, Merrick M (2005) *In vivo* functional characterization of the *Escherichia coli* ammonium channel AmtB: evidence for metabolic coupling of AmtB to glutamine synthetase. *Biochem J* 390: 215 – 222

Javelle A, Lupo D, Zheng L, Li XD, Winkler FK, Merrick M (2006) An unusual twin-his arrangement in the pore of ammonia channels is essential for substrate conductance. *J Biol Chem* 281: 39492 – 39498

Javelle A, Lupo D, Ripoche P, Fulford T, Merrick M, Winkler FK (2008) Substrate binding, deprotonation, and selectivity at the periplasmic entrance of the *Escherichia coli* ammonia channel AmtB. *Proc Natl Acad Sci USA* 105: 5040 – 5045

Jia W, Tovell N, Clegg S, Trimmer M, Cole J (2009) A single channel for nitrate uptake, nitrite export and nitrite uptake by *Escherichia coli* NarU and a role for NirC in nitrite export and uptake. *Biochem J* 417: 297 – 304

Khademi S, O'Connell J III, Remis J, Robles-Colmenares Y, Miercke LJ, Stroud RM (2004) Mechanism of ammonia transport by Amt/MEP/Rh: structure of AmtB at 1.35 Å. *Science* 305: 1587 – 1594

Kim YJ, Lee HS, Kim ES, Bae SS, Lim JK, Matsumi R, Lebedinsky AV, Sokolova TG, Kozhevnikova DA, Cha SS, Kim SJ, Kwon KK, Imanaka T, Atomi H, Bonch-Osmolovskaya EA, Lee JH, Kang SG (2010) Formate-driven growth coupled with H_2 production. *Nature* 467: 352 – 355

Lü W, Du J, Wacker T, Gerbig-Smentek E, Andrade SL, Einsle O (2011) pH-dependent gating in a FocA formate channel. *Science* 332: 352 – 354

Lü W, Du J, Schwarzer NJ, Gerbig-Smentek E, Einsle O, Andrade SL (2012a) The formate channel FocA exports the products of mixed-acid fermentation. *Proc Natl Acad Sci USA* 109: 13254 – 13259

Lü W, Schwarzer NJ, Du J, Gerbig-Smentek E, Andrade SL, Einsle O (2012b) Structural and functional characterization of the nitrite channel NirC from *Salmonella typhimurium*. *Proc Natl Acad Sci USA* 109: 18395 – 18400

Lü W, Du J, Schwarzer NJ, Wacker T, Andrade SL, Einsle O (2013) The formate/nitrite transporter family of anion channels. *Biol Chem* 394: 715 – 727

Lv X, Liu H, Ke M, Gong H (2013) Exploring the pH-dependent substrate transport mechanism of FocA using molecular dynamics simulation. *Biophys J* 105: 2714 – 2723

Marchetti RV, Lehane AM, Shafik SH, Winterberg M, Martin RE, Kirk K (2015) A lactate and formate transporter in the intraerythrocytic malaria parasite, *Plasmodium falciparum*. *Nat Commun* 6: 6721

McIlvaine TC (1921) A buffer solution for colorimetric comparison. *J Biol Chem* 49: 183 – 186

McLaughlin SGA, Dilger JP (1980) Transport of protons across membranes by weak acids. *Physiol Rev* 60: 825 – 863

Mertz EL, Krishtalik LI (2000) Low dielectric response in enzyme active site. *Proc Natl Acad Sci USA* 97: 2081 – 2086

Neuhäuser B, Dynowski M, Ludewig U (2014) Switching substrate specificity of AMT/MEP/Rh proteins. *Channels* 8: 496 – 502

Pettersen EF, Goddard TD, Huang CC, Couch GS, Greenblatt DM, Meng EC, Ferrin TE (2004) UCSF Chimera — a visualization system for exploratory research and analysis. *J Comput Chem* 25: 1605 – 1612

Sarmini K, Kenndler E (1999) Ionization constants of weak acids and bases in organic solvents. *J Biochem Biophys Methods* 38: 123 – 137

Sawers RG (2005) Formate and its role in hydrogen production in *Escherichia coli*. *Biochem Soc Trans* 33: 42 – 45

Sawers RG (2006) Differential turnover of the multiple processed transcripts of the *Escherichia coli* focA-pflB operon. *Microbiology* 152: 2197 – 2205

Song J, Baker N, Rothert M, Henke B, Jeacock L, Horn D, Beitz E (2016) Pentamidine is not a permeant but a nanomolar inhibitor of the *Trypanosoma brucei* aquaglyceroporin-2. *PLoS Pathog* 12: e1005436

Suppmann B, Sawers G (1994) Isolation and characterization of hypophosphite-resistant mutants of *Escherichia coli*: identification of the FocA protein, encoded by the pfl operon, as a putative formate transporter. *Mol Microbiol* 11: 965 – 982

Tan KP, Nguyen TB, Patel S, Varadarajan R, Madhusudhan MS (2013) Depth: a web server to compute depth, cavity sizes, detect potential small-molecule ligand-binding cavities and predict the pKa of ionizable residues in proteins. *Nucl Acids Res* 41: W314 – W321

Waight AB, Love J, Wang DN (2010) Structure and mechanism of a pentameric formate channel. *Nat Struct Mol Biol* 17: 31 – 37

Waight AB, Czyzewski BK, Wang DN (2013) Ion selectivity and gating mechanisms of FNT channels. *Curr Opin Struct Biol* 23: 499 – 506

Wang Y, Huang Y, Wang J, Cheng C, Huang W, Lu P, Xu Y-N, Wang P, Yan N, Shi Y (2009) Structure of the formate transporter FocA reveals a pentameric aquaporin-like channel. *Nature* 462: 467 – 472

Wu B, Rambow J, Bock S, Holm-Bertelsen J, Wiechert M, Soares AB, Spielmann T, Beitz E (2015) Identity of a *Plasmodium* lactate/H^+ symporter structurally unrelated to human transporters. *Nat Commun* 6: 6284

